Monte Carlo Simulation of Off-Lattice Polymer Chains: Effective Pair Potentials in Dilute Solution

James Dautenhahn and Carol K. Hall*

Department of Chemical Engineering, North Carolina State University, Raleigh, North Carolina 27695-7905

Received March 10, 1994; Revised Manuscript Received May 31, 1994®

ABSTRACT: Monte Carlo methods are used to calculate the mean squared radius of gyration, $\langle R_g^2 \rangle$, potential of mean force, $U(r)$, and second osmotic virial coefficient, B_2, of polymer chains. Two models of polymers as off-lattice chains of tangent hard spheres are used. In the first, the beads of the chains are simply hard spheres (the athermal case). In the second, the beads of the chains are allowed to interact with nonadjacent beads on the same chain and with beads on a different chain via a square-well potential. In both models, conformations of chains with 50, 100, 200, and 500 segments were generated. In the square-well model, square-well potentials $\epsilon = -0.15kT$, $-0.3kT$, and $-0.45kT$ were used. Examination of the radius of gyration of single chains shows a Θ-point (defined to be the temperature at which $\langle R_g^2 \rangle$ depends linearly on the chain length) at $\epsilon_\Theta \cong -0.32kT$. The radius of gyration of two interacting chains shows that as the chains are brought close together, they become compressed along the axis between their centers of mass and expanded perpendicular to this axis. The potential of mean force, $U(r)$, between two polymer chains is calculated as a function of the separation between the chains' centers of mass and is found to decrease as chain length increases. This is in contrast to the Flory–Krigbaum theory but is in agreement with previous findings of Grosberg et al. For chains of different lengths, $U(r)$ decreases as the difference between the lengths of the chains increases. Near the Θ-point, the $U(r)$ curves tend to be indistinguishable for all chain lengths. The second osmotic virial coefficient is calculated from the potential of mean force. Scaling analysis on the second osmotic virial coefficient for athermal chains gives a scaling exponent of $\gamma = 0.272 \pm 0.005$, in agreement with the findings of Yethiraj et al. The Θ-point (defined here as the point where $B_2 = 0$) is found to be at a square-well potential of $\epsilon_\Theta \cong -0.32kT$. This is the same as the Θ-point defined in terms of the radius of gyration and is in agreement with the results of Wichert and Hall. A correlation for $U(r)$ that fits the simulation data reasonably well is also presented.

1. Introduction

This paper presents Monte Carlo calculations of the effective polymer–polymer potential, the second osmotic virial coefficient, and the radius of gyration for off-lattice polymer chains. The primary aim of this work is to develop functional forms for the potential of mean force between polymer molecules in dilute solution which can then be used in the development of theories which describe aqueous two-phase polymer solutions. The motivation for this work is our long-term goal of developing a theory which describes the partitioning of proteins between the phases formed when two different polymers are mixed in aqueous solution. In developing such a theory, we are immediately faced with the problem of simultaneously modeling proteins, which are best treated on the molecular level, and polymers, which are best treated on the segment level. Our solution to this problem is to convert the segment-level description of polymer chains to a molecular-level description by calculating the effective interaction potential (or potential of mean force) between two polymer chains. In this paper we describe our calculation of this effective pair potential using Monte Carlo methods. A subsequent paper will be devoted to calculating the effective pair potential between a polymer chain and a protein molecule.

In the work presented in this paper, we investigate the radius of gyration, potential of mean force, and second osmotic virial coefficient of polymer chains in dilute solution. There have been a number of computer simulation investigations of these three properties; however, most of these studies have been restricted to lattice chains. A short review of those studies which are relevant to this work is presented here.

The radius of gyration (or, equivalently, the end-to-end distance) for single lattice chains has been studied by many groups, most recently by Bishop and Clarke[1] and by Yuan and Masters.[2] The work of Yuan and Masters is relevant to our study because it also examines the Θ-point, which can be defined as the temperature at which the radius of gyration is directly proportional to the chain length. Some early work by Olaj and Lantschbauer[3] examines the radius of gyration of both on-lattice and off-lattice chains, but the work is limited to athermal chains. Olaj et al.[4,5] also examine how the radius of gyration changes as two lattice chains are brought close together. By looking at how the components of the radius of gyration parallel and perpendicular to the axis between the chains' centers of mass change as the chains are brought close together, we gain insight into how the changing shape of the chains affects the potential of mean force.

As previously stated, the primary aim of this work is to develop a functional form for the potential of mean force between polymer molecules in dilute solution. There have been relatively few computer simulation studies of the potential of mean force, $U(r)$ (or, equivalently, the pair distribution function, $G(r) = \exp^{-U(r)}$). Olaj and Pelinka[6] report $G(r)$ for nonathermal lattice chains. Additionally, Olaj and Lantschbauer[3] report $G(r)$ for both on-lattice and off-lattice athermal chains, but the simulations of off-lattice chains were never extended to include interactions between beads of the chains. Grosberg et al.[7] and Krüger et al.[8] both present data on $G(r)$ for off-lattice athermal chains; however, the Krüger et al. model differs from the one used in our study in that it uses hard-sphere segments joined by rigid rods rather than tangent hard spheres, making the model resemble a lattice chain. The Grosberg et al. model, however, is the same as ours. We will see that the $G(r)$ results of Olaj and Lantschbauer[3] and of Grosberg

® Abstract published in *Advance ACS Abstracts*, August 1, 1994.

0024-9297/94/2227-5399$04.50/0

et al.[7] are in agreement with our $U(r)$ results for athermal off-lattice chains.

Since the studies described above examine only athermal chains, we cannot use them to check our simulation results on interacting chains. We can, however, compare our results on interacting chains to theoretical treatments of $U(r)$. Since Flory and Krigbaum[9] first proposed their theory of dilute polymer solutions, various approaches[10-13] have been taken to refine their equation for $U(r)$. A common approach is that of Czech and Hall,[14] who added extra terms to the Flory–Krigbaum equation in order to correct it for the collapse of polymer chains near the Θ-point. We find, however, that equations of this type do not fit our simulation data very well. Another approach to solving this problem is that of Olaj et al.[6,15,16] who have modeled $U(r)$ near the Θ-point by separating the attractive and repulsive interactions of the chains into two terms. Although this gives reasonable fits of data near the Θ-point, it does not work very well for athermal chains.

The second osmotic virial coefficient can be calculated directly from $U(r)$, giving us another way of comparing our results to those already reported. The second osmotic virial coefficient and the Θ-point, defined as the temperature at which the second osmotic virial coefficient is zero, have been calculated in several studies of lattice chains,[17-25], including one by Barrett[21] which examines the second osmotic virial coefficient between chains of different lengths. Of greater relevance to this work, however, are the off-lattice results of Yethiraj et al.,[26] who examine the scaling of the second osmotic virial coefficient for long athermal chains, and Wichert and Hall,[27] who examine the second osmotic virial coefficient and Θ-point for chains that have attractive potentials. Both of these studies use the same model as ours; our results are in good agreement with these studies. Hopefully, the work presented in this paper will fill in some of the gaps in this body of knowledge and will aid in the development of new theoretical treatments of this problem.

In this paper, two models of a polymer chain are considered: athermal chains and chains with attractive potentials. In the athermal chain model, the polymer is treated as a chain of tangent hard spheres of unit diameter which are allowed to be in any conformation which does not result in bead overlap. In the attractive interaction model, the polymer is treated in the same manner with the exception that nonadjacent beads on the same chain and beads on different chains interact via a square-well potential with well depth $\epsilon = 0.15kT$, $-0.3kT$, or $-0.45kT$ and well width $\lambda = 0.5$. Single chains are generated using the pivot algorithm, each Monte Carlo step is a rotation of one end of the chain about a randomly selected pivot point to a new position. Pairs of chains generated by this method are then placed in a box with their centers of mass at various separations. By checking the beads of the chains for overlaps and, in the case of square-well chains, for beads falling in the attractive well, the potential of mean force between the chains can be calculated. In this manner, the properties of single chains and pairs of chains can be examined.

Results from the computer simulations are presented in three forms: the radius of gyration, R_g, of the chain; the potential of mean force, $U(r)$, between two chains; and the second osmotic virial coefficient, B_2. The radius of gyration is used to measure the size and shape of the polymer chains. It is found that as the chains are brought closer together they become compressed along the axis between their centers of mass and expanded in directions perpendicular to this axis. Once the chains penetrate each other, they expand in all directions to create space for each other. The potential of mean force between two chains is calculated as a function of the distance between the centers of mass of the two chains. For chains of equal length, the potential of mean force is found to decrease as the chains increase in length. This is contrary to the Flory–Krigbaum theory[9] prediction, which says that $U(r)$ increases with chain length, but is reasonable considering that longer chains can more easily penetrate each other. The potential of mean force between chains of different lengths is found to be lower than the potential of mean force between chains of the same length. In addition, the potential of mean force decreases as the difference in the length of the chains increases. Again, this is reasonable because a smaller chain can penetrate a larger chain more easily than it can penetrate a chain of the same length. A correlation which fits the simulation data for $U(r)$ reasonably well is also developed. The second osmotic virial coefficient is calculated by integrating a function of the potential of mean force (given later in this paper) over all distances. The results of these calculations give a Θ-point (the point where $B_2 = 0$) at a bead–bead interaction potential $\epsilon_\Theta \cong -0.32kT$. Another definition of the Θ-point for polymer collapse is when $R_g^2 \propto n$ (chain length). This is also seen to occur at $\epsilon_\Theta \cong -0.32kT$. This shows that for off-lattice chains the two Θ-point definitions are equivalent.

The rest of this paper is organized as follows. In section 2, the Monte Carlo method used to generate single chain conformations and the procedure used to calculate $U(r)$ are described in detail. Section 3 presents the results of the simulations for the radius of gyration, R_g, the potential of mean force, $U(r)$, and the second osmotic virial coefficient, B_2. Section 4 presents a correlation for $U(r)$ that does a reasonable job of fitting the simulation data. Section 5 summarizes our findings and what was learned from the results.

2. Monte Carlo and Computer Methods

The Monte Carlo method described below was used to simulate polymer chains in dilute solution. First, single polymer chain conformations were generated using the pivot algorithm. Hard-sphere (athermal) chains of length $n = 50$, 100, 200, and 500 beads were generated. Square-well chains of length $n = 50$, 100, and 200 were generated for bead–bead interaction potentials $\epsilon = -0.15kT$, $-0.3kT$, and $-0.45kT$, at a single well width $\lambda = 0.5$, where k is Boltzmann's constant and T is the temperature. (It should be noted here that the solvent molecules, which are assumed to completely surround the polymer chains, are not explicitly taken into account with this model. Thus, the bead–bead interaction potentials, ϵ, should be considered potentials of mean force between beads rather than potential energies.) Pairs of these single chains were then placed with their centers of mass at various distances, effectively creating two-chain configurations. From these pairs of chains the potential of mean force between the two chains was calculated as a function of the distance between their centers of mass. The potential of mean force was then used to calculate the second osmotic virial coefficient.

The pivot algorithm is used to generate single chain conformations for both hard-sphere and square-well chains. In the pivot algorithm, one bead on a chain is randomly selected to be the pivot point. The short end of the chain is then rigidly rotated through a randomly selected angle to a new position. The new conformation is then checked for overlap. If any of the beads overlap, the move is rejected and a new pivot point on the original

conformation is selected for a trial rotation. If no beads overlap, then the probability, $P_{1\to2}$, of accepting the move depends on the intramolecular potentials of the initial and final conformations in the following manner:

$$P_{1\to2} = \exp^{-E_2/kT}/\exp^{-E_1/kT} \tag{1}$$

where E_1 and E_2 are the intramolecular potentials of the initial and final conformations, respectively. This is implemented on the computer by comparing $P_{1\to2}$ with a random number, x, between 0 and 1. If $P_{1\to2} > x$, then the move is accepted and the new conformation is used for the next attempted move; if not, the original conformation is used again. For the hard-sphere case (athermal chains), the move is always accepted if there is no overlap, since $P_{1\to2} = 1$. For the square-well chains, the intramolecular potential is the bead–bead interaction potential times the number of pairs of beads in an attractive well. Thus, if the new conformation has more pairs of beads in the attractive well than the previous conformation and hence is energetically more favorable, then the move is accepted, since $P_{1\to2} > 1$. This method, which is essentially the Metropolis algorithm, allows a chain to "back out" of high-energy conformations by permitting energetically less favorable moves to be accepted occasionally. In this fashion, distinct sets of single chain conformations were generated.

The average interaction energy between chains, $U(r)$, is determined using two sets of single chain conformations in the following manner. Two chains, one from each set of conformations, are placed at random relative orientations with their centers of mass a given distance apart. The distance between the centers of mass of the two chains is varied from 0 to 5 times the average radius of gyration of the two chains (far enough apart that the two chains do not interact) with 26 intervals between. All possible pairs of configurations are considered. At each separation between the centers of mass, the beads on the pair of chains are checked for overlap and, in the case of square-well chains, for attractive intermolecular interaction. The statistical weight of each configuration at a given separation is calculated using the following equation:

$$W_i(r) = \exp^{-\phi_i(r)/kT} \tag{2}$$

where $W_i(r)$ is the weighting of the two-chain configuration i, r is the distance separating the centers of mass of the two chains, and $\phi_i(r)$ is the potential between the two chains in configuration i. The potential of mean force between the chains, $U(r)$, is then calculated as a function of the distance of separation between the two centers of mass using the following equation:

$$\frac{U(r)}{kT} = -\ln \frac{\sum_{i=1}^{M} W_i(r)}{M} \tag{3}$$

where M is the total number of two chain configurations used at that distance. For hard-sphere (athermal) chains, this calculation is rather simple. If there is no overlap between the two conformations, then the potential between the two chains $\phi_i(r) = 0$ and the statistical weight of the configuration $W_i(r) = 1$. If the two chains overlap, $\phi_i(r) = \infty$ and $W_i(r) = 0$. Thus, the average weighting used to calculate $U(r)$ for athermal chains is merely the fraction of two-chain configurations that do not overlap. For the case of square-well chains, the potential between two nonoverlapping chains in configuration i is given by $\phi_i(r) = N_p^{(i)}(r)\epsilon$ where $N_p^{(i)}(r)$ is the number of pairs of beads (one from each chain) in the interactive well and ϵ is the bead–bead pair potential. Again, for this case, if the chains overlap, $\phi_i(r) = \infty$ and $W_i(r) = 0$.

Table 1. Number of Single Chain Conformations and Radius of Gyration

n	$-\epsilon/kT$	conformations/10^6	$\langle R_g^2 \rangle$
10	0.0	5.01	2.858 ± 0.006
20	0.0	5.02	7.26 ± 0.01
25	0.0	5.025	9.74 ± 0.02
40	0.0	5.04	17.90 ± 0.06
50	0.0	18.125	23.74 ± 0.04
100	0.0	7.6	56.6 ± 0.1
200	0.0	10.2	132.3 ± 0.4
500	0.0	15.625	402 ± 1
1000	0.0	13.0	918 ± 3
50	0.15	5.0	20.89 ± 0.08
100	0.15	5.0	48.9 ± 0.3
200	0.15	5.9	113.1 ± 0.4
500	0.15	5.0	338 ± 2
50	0.3	8.425	16.84 ± 0.08
100	0.3	16.4	36.9 ± 0.2
200	0.3	8.8	81.1 ± 0.9
500	0.3	10.3125	227 ± 4
50	0.45	22.4	11.1 ± 0.1
100	0.45	21.0	18.8 ± 0.4
200	0.45	24.5	25 ± 2
500	0.45	20.0	39.5 ± 0.4

The pivot algorithm described above was implemented in the following manner. The pivot algorithm was used to determine the mean squared radius of gyration, $\langle R_g^2 \rangle$, and the fraction of attempted moves which were accepted. The radius of gyration was used for two distinct purposes. First, from examining the dependence of $\langle R_g^2 \rangle$ on chain length, the Θ-point (defined as the ϵ where $\langle R_g^2 \rangle \propto n$) was determined. Second, as mentioned before, when $U(r)$ is calculated, the two chains are placed at a maximum distance of 5 times the average radius of gyration of the two chains (since the two chains will be far enough apart that they will not interact). The acceptance fraction was used to determine the number of attempted moves to make in order to obtain a given number of independent conformations; an independent conformation is generated after a number of accepted pivot algorithm moves equal to the chain length.[28] Once the acceptance fraction was known, distinct sets of single chain conformations containing 750 conformations for $n = 50$, $n = 100$, and $n = 200$ and 250 conformations for $n = 500$ were generated for use in calculating $U(r)$. For example, to generate 750 conformations of chains of 50 segments at $\epsilon = 0.0$, which had an acceptance fraction of 0.65, we needed to attempt $750 \times 50/0.65 \simeq 57\,692$ moves. To be on the safe side, in this case we attempted 75 000 moves and saved every $^1/_{100}$th conformation. Table 1 gives the total number of conformations (attempted moves) for initial runs used to determine the acceptance fraction and radius of gyration and for runs which generated the sets of conformations used to calculate $U(r)$. Table 1 also shows the mean squared radius of gyration and its standard error for each case examined. For example, for $n = 50$ at $\epsilon = 0.0$ a total of 18.125 million moves were attempted and the resulting conformations had a mean squared radius of gyration $\langle R_g^2 \rangle = 23.74 \pm 0.04$.

Two sets of single chain conformations were then used to calculate $U(r)$, as described earlier. Comparing each conformation from one set with each conformation from another set gave 62 500 (for $n_1 = n_2 = 500$) to 562 500 (for $n_1 = n_2 = 50$) two-chain configurations. Error estimates for the properties examined in all of these calculations

Table 2. Number of Two-Chain Configurations Used To Calculate $U(r)$

			configurations/10^6		
n_1	n_2	$-\epsilon/kT$	for large r	for small r	at $r = 0$
50	50	0.0	0.5625	0.5625	8.5625
50	50	0.15	0.5625	0.5625	
50	50	0.3	0.25	9.5	
50	50	0.45	0.25	71.5	
100	100	0.0	0.5625	0.5625	8.5625
100	100	0.15	0.5625	0.5625	
100	100	0.3	0.25	18.75	
200	200	0.0	0.5625	0.5625	8.5625
200	200	0.15	0.5625	0.5625	
200	200	0.3	0.25	1.25	
500	500	0.0	0.0625	0.0625	4.0625
1000	1000	0.0			0.75
50	25	0.0	0.25	0.25	
100	50	0.0	0.5625	0.5625	
100	50	0.15	0.25	0.25	
100	50	0.3	0.25	4.5	
200	100	0.0	0.125	0.125	
200	100	0.15	0.125	0.125	
200	100	0.3	0.125	2.375	
50	10	0.0	0.25	0.25	
100	20	0.0	0.25	0.25	
200	40	0.0	0.25	0.25	
500	100	0.0	0.3125	0.3125	
500	100	0.15	0.3125	0.3125	
500	100	0.3	0.0625	4.5625	

were obtained by calculating an average value for each batch and using the standard error formula:

$$s = \left(\frac{\sum_{i=1}^{N_b} A_{bi}^2}{N_b} - A_{tot}^2 \right)^{1/2} \quad (4)$$

where s is the standard error, N_b is the number of batches, A_{bi} is the average value for batch i, and A_{tot} is the average value over all batches. For the more attractive square-well chains ($\epsilon = -0.3kT$ and $\epsilon = -0.45kT$), the standard error calculated in this manner was often quite large at small distances of separation between the centers of mass of the two chains. To reduce the standard error in these cases, additional sets of conformations were generated to provide more two-chain configurations at short distances. For example, in the case of $n_1 = n_2 = 50$ at $\epsilon = -0.3kT$ a total of 9.5 million two-chain configurations were used at small separations to reduce the standard error of the observations. The large standard error in these strongly attractive cases was due to the fact that only a few high-energy configurations contribute significantly to the average properties. Table 2 gives the range of the number of two-chain configurations used for large and small r for all combinations of n_1, n_2, and ϵ that were examined. Table 2 also gives the number of two-chain configurations used at $r = 0$ for athermal chains of the same length. These simulations were designed to calculate $U(r = 0)$ to a high degree of accuracy for use in developing a correlation for $U(r)$. Note that the error bars have been omitted from all the figures unless they were larger than the symbols representing the data. The standard error was calculated for all of the data shown in the figures. The results of our computer simulations are presented in the next section.

3. Results

The results obtained from our computer simulations for the radius of gyration, R_g, of both single chains and pairs of chains, the potential of mean force, $U(r)$, between two chains, and the second osmotic virial coefficient, B_2, are presented in this section. Since the radius of gyration is a measure of the size of a polymer chain and is often used to scale results for different length chains, it will be examined first.

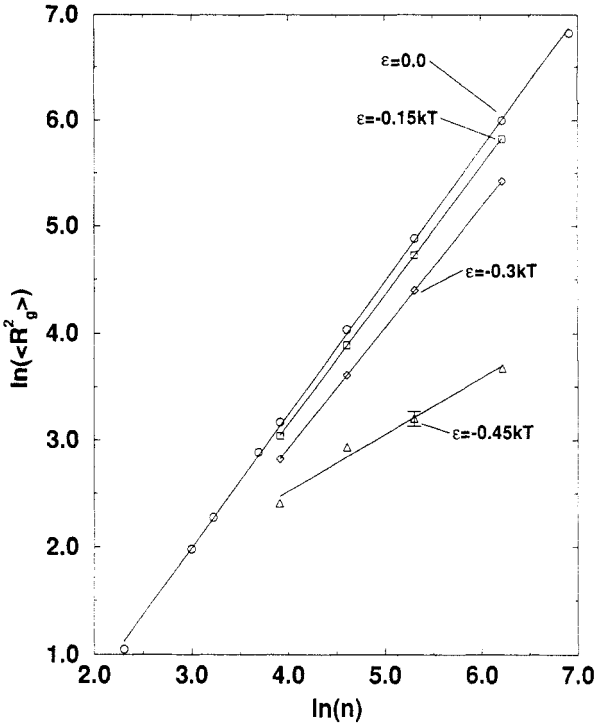

Figure 1. Radius of gyration of single chains vs chain length: (○) athermal, (□) $\epsilon = -0.15kT$, (◇) $\epsilon = -0.3kT$, and (△) $\epsilon = -0.45kT$. Lines are linear fits to data for each ϵ.

The radius of gyration of a single chain, R_g, is calculated by evaluating the distance of the beads along the chain from the chain's center of mass in the following manner

$$R_g^2 = \frac{1}{n}\sum_{i=1}^{n}((x_i - x_{cm})^2 + (y_i - y_{cm})^2 + (z_i + z_{cm})^2) \quad (5)$$

where n is the chain length; x_i, y_i, and z_i are the coordinates of bead i; and x_{cm}, y_{cm}, and z_{cm} are the coordinates of the chain's center of mass. Figure 1 shows the mean squared radius of gyration, $\langle R_g^2 \rangle$, versus n on a log–log scale for square-well depths $\epsilon = 0.0, -0.15kT, -0.3kT$, and $-0.45kT$. The number of conformations used for each point is given in Table 1, along with the actual values for $\langle R_g^2 \rangle$ and their standard error. The lines on the figure are linear fits to the simulation data at each ϵ. For any given ϵ, $\ln \langle R_g^2 \rangle$ has a linear dependence on $\ln n$, i.e. $\ln \langle R_g^2 \rangle \propto a \ln n$, where a is the slope of the line. As seen in the figure, the slope decreases as the well depth increases. The Θ-point is the temperature (or ϵ) at which $\langle R_g^2 \rangle$ depends linearly on n, i.e. when the slope of the line in Figure 1 is unity. Interpolating between the slopes of the lines on the figure, it is found that the Θ-point ($a = 1$) is at $\epsilon_\Theta \cong -0.32kT$. This result agrees with other simulations for short ($n \leq 16$) off-lattice chains done by our group[27] using the same model. Comparison of Θ-point results to lattice chain results is not particularly useful. For lattice chains, the coordination number of the lattice determines the Θ-point.[6] For off-lattice chains, the well width ($\lambda = 0.5$ for our simulations) would determine the Θ-point. As the well width is increased, the bead–bead attraction at the Θ-point will decrease (ϵ_Θ will move closer to zero).

The radius of gyration can be used to determine how the size and shape of two chains change as a function of

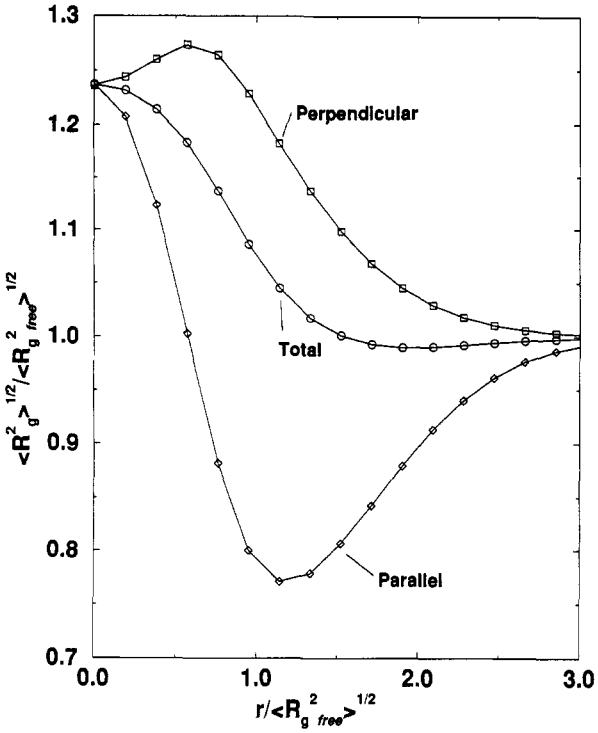

Figure 2. Radius of gyration for interacting athermal chains (n = 50) vs distance between the centers of mass: (○) $\langle R_g^2\rangle^{1/2}$, (□) component perpendicular to axis between centers of mass, and (◇) component parallel to axis between centers of mass.

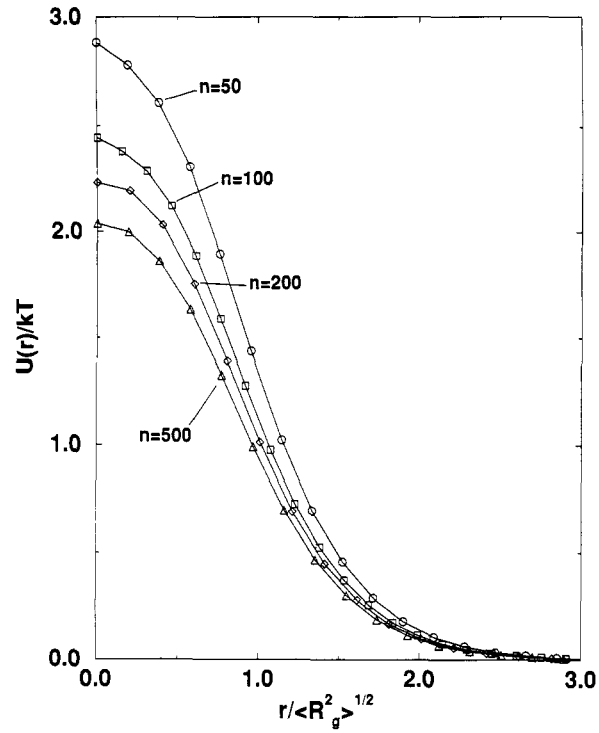

Figure 3. $U(r)$ for athermal chains of the same length: (○) n = 50, (□) n = 100, (◇) n = 200, and (△) n = 500.

the distance of separation between their centers of mass. The size is measured by the chain's radius of gyration, R_g, while the shape is measured by determining the components of R_g perpendicular and parallel to the axis between the centers of mass. Figure 2 shows the root mean squared radius of gyration ($\langle R_g^2\rangle^{1/2}$) for athermal chains along with its perpendicular and parallel components as a function of the distance of separation for like polymers (n = 50). The changes in these properties with the distance of separation is determined by calculating the weighted average (using the configurational statistical weight described earlier in eq 2) of the single chain properties. The radius of gyration is normalized by the average single chain radius of gyration, while the perpendicular and parallel components are normalized by their values at an infinite distance of separation. From the figure, it can easily be seen that as the chains are brought closer, the average size of the chains decreases slightly but that the shape of the chains changes dramatically. The chains become compressed along the axis between the centers of mass and expanded perpendicular to the axis as the chains try to avoid interfering with each other. As the chains move even closer together, the size increases dramatically, since larger chains are more spread out and have more open space to accommodate the beads of the other chain. Finally, when the centers of mass coincide, the normalized properties all have the same value, indicating that there is no longer any difference between perpendicular and parallel components. These results are consistent with those reported by Olaj et al.[4,5] for lattice chains. Later we will see that knowledge of the changes in the chains' shape and size with interchain separation is critical in understanding our potential of mean force results.

The potential of mean force, $U(r)$, between two chains is calculated as described in the previous section. Figure 3 shows a plot of $U(r)$ versus the distance between the centers of mass of the two chains for athermal (hard-sphere) chains of the same length n = 50, 100, 200, and 500. The distance is normalized by the root mean squared radius of gyration of the free single polymer chains. There is no attractive potential between the chains. As the chains are brought together, there is a repulsion but the repulsion does not go to infinity even when the chain centers of mass coincide. This is because the chains are able to penetrate each other at short distances of separation. As we saw in Figure 2, chains become compressed parallel to the axis between the centers of mass and expanded perpendicular to it, and as the centers of mass begin to coincide, the chains expand in all directions to accommodate each other. This mutual accommodation of chains shows why $U(r)$ decreases with increasing chain length. Longer chains are able to spread out further from their centers of mass, thus being more penetrable. Again, it should be noted that this result is in contrast to the Flory–Krigbaum theory,[9] which says that $U(r)$ increases with increasing chain length. However, our results agree with the previous findings of Grosberg et al.[7] and seem reasonable considering how the size and shape of the two chains change as they are brought close together. Comparing our results on $U(r)$ to results on $G(r) = \exp^{-U(r)}$ by both Olaj and Lantschbauer[3] for n = 50 and Grosberg et al.[7] for $30 \le n \le 100$ shows that the resulting curves are essentially the same.

Figure 4 shows $U(r)$ between an athermal chain of length n_1 = 100 and chains of length n_2 = 50, 100, 200, and 500. The distance is normalized by the root average mean squared radius of gyration of the two free single polymer chains, $[(\langle R_{g1}^2\rangle + \langle R_{g2}^2\rangle)/2]^{1/2}$. It can be seen that when the chains are of different lengths, $U(r)$ is smaller than when the chains are of the same length. Further, comparison of Figures 3 and 4 shows that $U(r)$ decreases as the difference in length becomes larger. That is, the $U(r)$ curve for the n_1 = 100, n_2 = 50 case in Figure 4 is only slightly below that of the $n_1 = n_2$ = 100 case in Figure 3 (which is repeated in Figure 4). Likewise, although the n_1 = 100, n_2 = 200 case in Figure 4 is slightly lower than the $n_1 = n_2$ = 200 case in Figure 3, the n_1 = 100, n_2 = 500 case in Figure 4 is much lower than the $n_1 = n_2$ = 500 case in Figure 3. Again, this is the result of the chains being

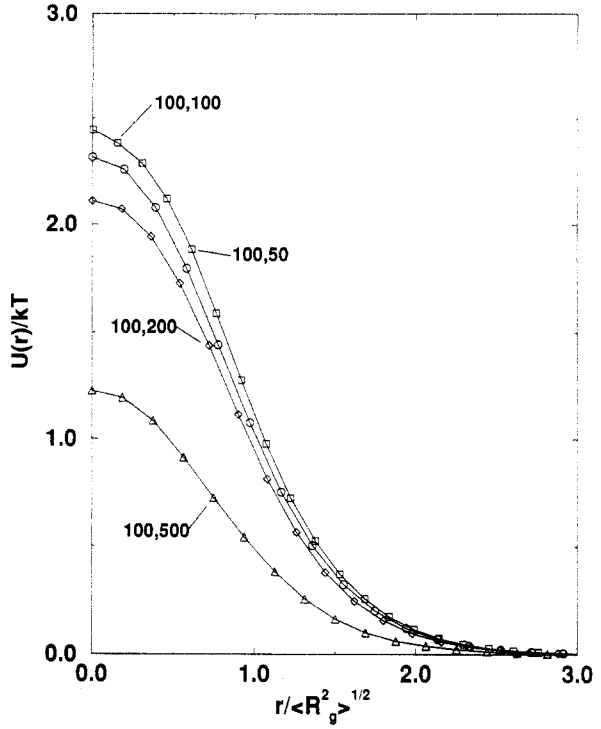

Figure 4. $U(r)$ for athermal chains of different lengths with n_1 = 100: (○) n_2 = 50, (□) n_2 = 100, (◇) n_2 = 200, and (△) n_2 = 500.

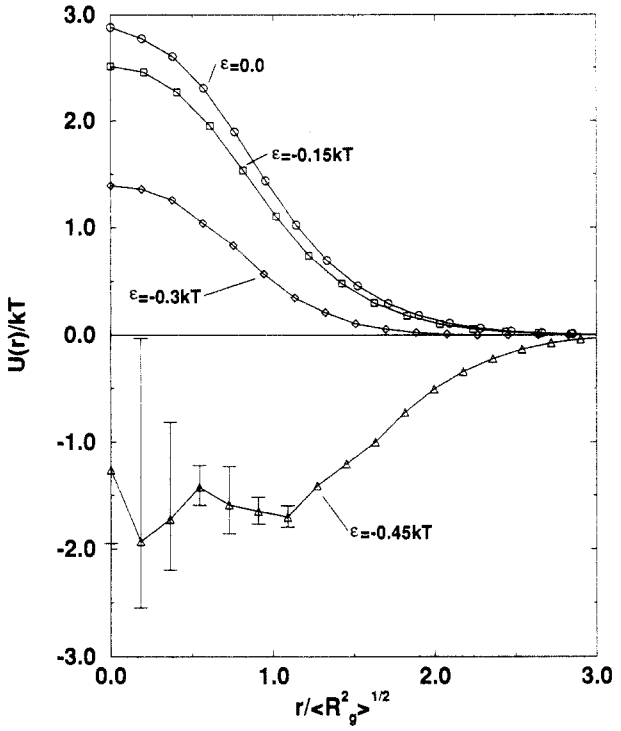

Figure 5. $U(r)$ for chains of length n = 50 for varying well depth ϵ: (○) athermal, (□) $\epsilon = -0.15kT$, (◇) $\epsilon = -0.3kT$, and (△) $\epsilon = -0.45kT$.

better able to penetrate one another when one of them is smaller. If the chains are of the same length (size), then they take up the same amount of space and are thus hard to fit together at small distances. However, if the chains are of different sizes, then it becomes easier to fit the smaller chain inside the larger chain as the centers of mass get closer.

Figure 5 shows $U(r)$ for chains of the same length (n = 50) with bead–bead interaction potentials of ϵ = 0.0, $-0.15kT$, $-0.3kT$, and $-0.45kT$. The standard error is significantly larger than the symbol size only for the $\epsilon = -0.45kT$ case. It can be seen that $U(r)$ decreases as ϵ decreases. This is expected; as the attraction between beads becomes greater, the chains can be brought close together more easily. As ϵ decreases to $-0.3kT$, the repulsion between chains at short distances decreases and there is even a slight attraction at longer distances. This is the same behavior noticed by Olaj and Pelinka[6] for lattice chains near the Θ-point. Finally, at $\epsilon = -0.45kT$, the chains are strongly attracted to each other, as evidenced by the negative potential between chains at all distances. The large standard error and nonsmoothness of the $\epsilon = -0.45kT$ curve are due to the fact that at small distances the fraction of two-chain configurations that do not overlap is very small and the ones that do not overlap are very high energy configurations. Thus, even though over 70 million configurations have been examined for the small separations, the $U(r)$ values shown are not particularly accurate. The $U(r)$ results are in keeping with the idea of good and bad solvents, which can be defined in terms of the Θ-point. Since the Θ-point is $-0.32kT$, good solvents are those for which $\epsilon > -0.32kT$ and bad solvents are those for which $\epsilon < -0.32kT$. (Note that although our simulations do not include solvent molecules, their interaction with the polymer chains is effectively accounted for by changing the well depth, ϵ. In our model, the polymer–solvent and solvent–solvent interactions are both taken to be zero and the polymer chains are assumed to be surrounded by solvent molecules. Thus, ϵ can be viewed as the polymer–polymer potential modified by polymer–solvent and solvent–solvent interactions. In essence, changing the solvent would change ϵ for a given polymer.) In good solvents (ϵ = 0.0 and $-0.15kT$), polymers prefer to be surrounded by solvent molecules and will repel each other. In Θ-solvents, polymers will repel each other at short distances but attract each other at longer distances, as evidenced by the near Θ-solvent ($\epsilon = -0.3kT$) data. In bad solvents ($\epsilon = -0.45kT$), polymers prefer to be surrounded by other polymers. This is evidenced by both the collapse of the single polymer chains, as seen in Figure 1, and the attractive well in $U(r)$ between two chains. The same trend is seen in longer chains.

Figures 6 and 7 show $U(r)$ for chains of length $n_1 = n_2$ = 100 and $n_1 = n_2$ = 200, respectively, for ϵ = 0.0, $-0.15kT$, and $-0.3kT$. Once again the standard error is given by the error bars. The same trends that were described for Figure 5 are also seen in Figures 6 and 7. $U(r)$ decreases as ϵ decreases. Thus, it is easier to bring the chains close together when the beads attract each other.

Figures 8 and 9 show $U(r)$ at $\epsilon = -0.15kT$ and $\epsilon = -0.3kT$, respectively, for chains of length n = 50, 100, and 200. The standard error is given by the error bars. As is seen in Figure 3 for athermal chains, $U(r)$ decreases as n increases in Figure 8 ($\epsilon = -0.15kT$). Once again, this is due to the fact that larger chains have more open space and can more easily penetrate each other. However, in Figure 9 there is very little difference among the curves. The $U(r)$ curves for n = 100 and 200 are nearly identical while that for n = 50 is slightly higher at short distances. This is not unusual, as we are close to the Θ-point ($\epsilon_\Theta \cong -0.32kT$) and we would expect the curves to converge.

Figure 10 shows $U(r)$ between a chain of length n_1 = 100 and chains of length n_2 = 50, 100, 200, and 500 at $\epsilon = -0.15kT$. The distance is normalized by the root average mean squared radius of gyration of the two chains, $[(\langle R_{g1}^2\rangle + \langle R_{g2}^2\rangle)/2]^{1/2}$. As was shown in Figure 4 for athermal chains, Figure 10 shows that for chains of different lengths, but with the same attractive interaction, $U(r)$ is smaller than when the chains are of the same length. Again, this

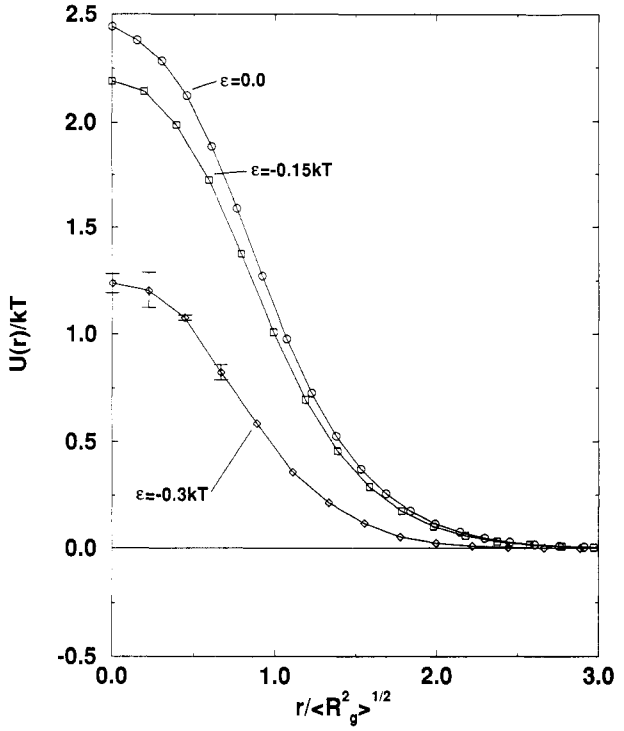

Figure 6. $U(r)$ for chains of length n = 100 for varying well depth ϵ: (○) athermal, (□) $\epsilon = -0.15kT$, and (◇) $\epsilon = -0.3kT$.

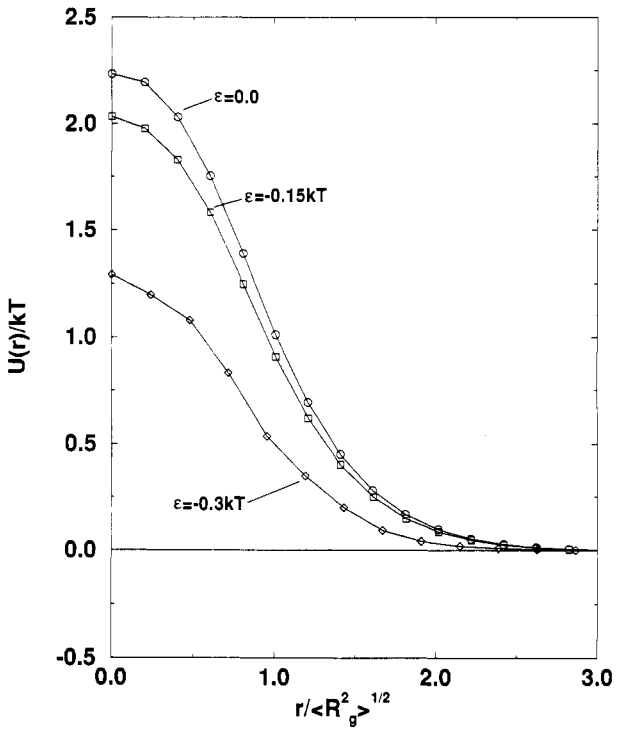

Figure 7. $U(r)$ for chains of length n = 200 for varying well depth ϵ: (○) athermal, (□) $\epsilon = -0.15kT$, and (◇) $\epsilon = -0.3kT$.

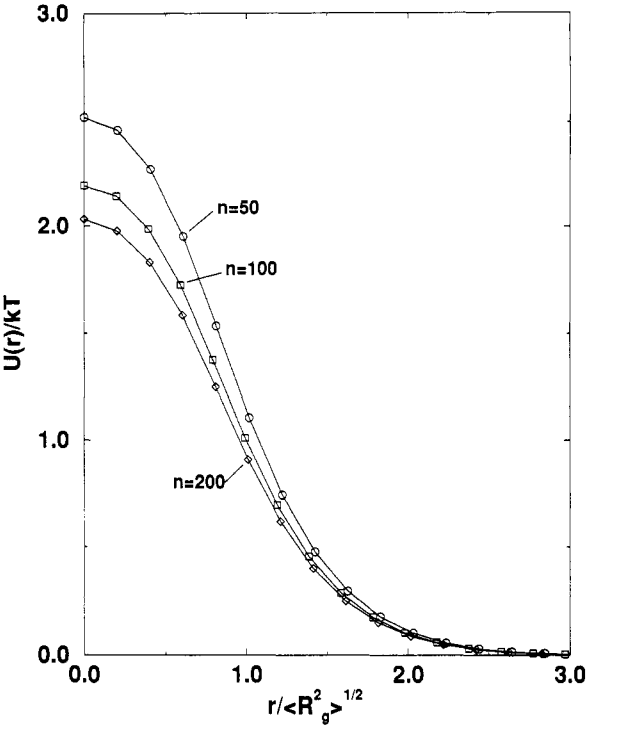

Figure 8. $U(r)$ for chains of the same length with $\epsilon = -0.15kT$: (○) n = 50, (□) n = 100, and (◇) n = 200.

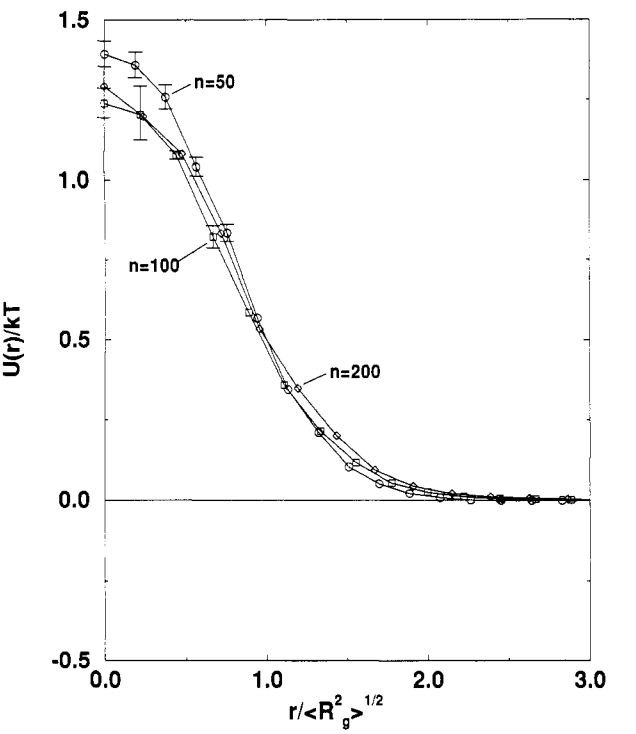

Figure 9. $U(r)$ for chains of the same length with $\epsilon = -0.3kT$: (○) n = 50, (□) n = 100, and (◇) n = 200.

is the result of the chains being better able to penetrate each other when one of the chains is smaller. The $U(r)$ curves in Figure 10 can also be seen to fall below those shown in Figure 4 for athermal chains. As is seen for chains of the same length in Figures 5 and 6, the attraction between beads of the chains enables them to be brought close together more easily.

Figure 11 shows $U(r)$ between a chain of length n_1 = 100 and chains of length n_2 = 50, 100, 200, and 500 at $\epsilon = -0.3kT$. Again the distance is normalized by the root average mean squared radius of gyration of the two chains (described previously for Figure 10) and the standard error is given. Comparing Figures 10 and 11 shows that $U(r)$ for unlike chains at $\epsilon = -0.3kT$ is lower than at $\epsilon = -0.15kT$. Again, the greater the interaction between beads of the chains, the easier it is to bring the chains close together. In addition, as seen in Figure 9 for chains of the same length at $\epsilon = -0.3kT$, the curves in Figure 11 also converge due to the fact that the Θ-point ($\epsilon_\Theta \cong -0.32kT$) is being approached. However, in this case there is a competing effect which keeps the curves somewhat separate. When the chains are of different sizes, $U(r)$ is smaller than when the chains are of the same size. It appears as though the ratio of the sizes has an effect on the values of $U(r)$ since

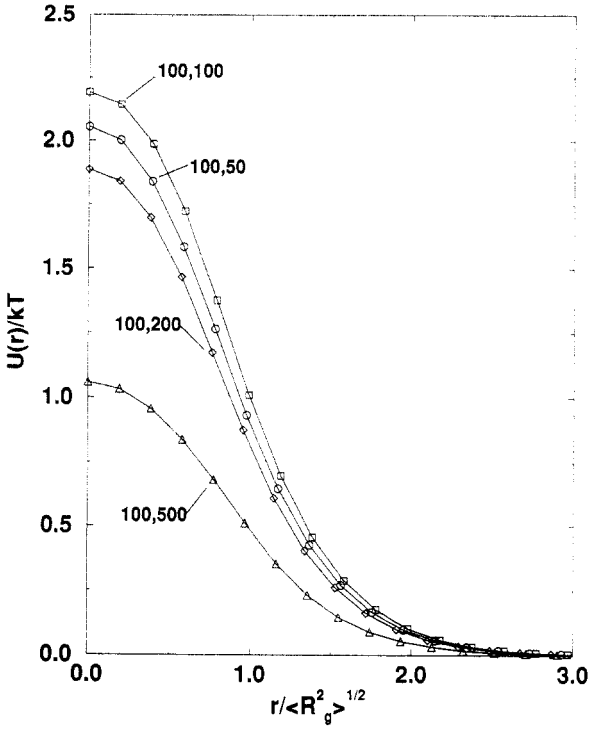

Figure 10. $U(r)$ for chains of different lengths with $n_1 = 100$ and $\epsilon = -0.15kT$: (○) $n_2 = 50$, (□) $n_2 = 100$, (◇) $n_2 = 200$, and (△) $n_2 = 500$.

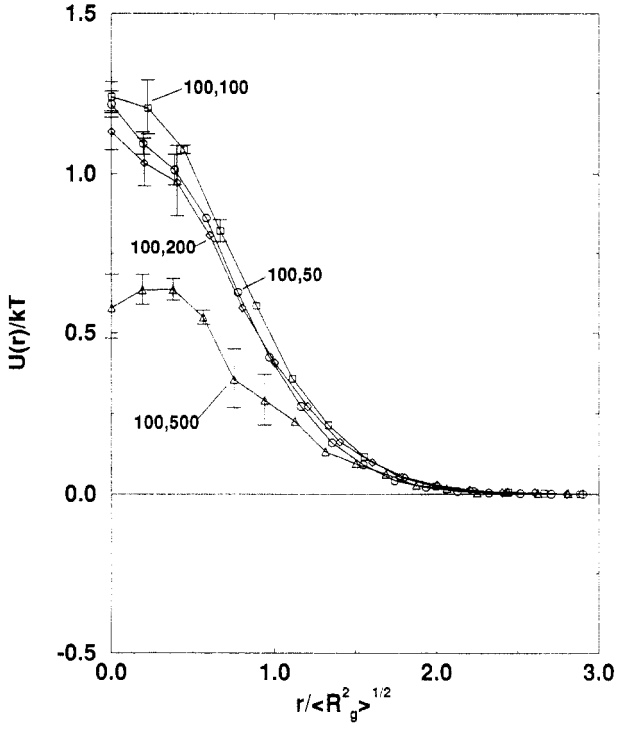

Figure 11. $U(r)$ for chains of different lengths with $n_1 = 100$ and $\epsilon = -0.3kT$: (○) $n_2 = 50$, (□) $n_2 = 100$, (◇) $n_2 = 200$, and (△) $n_2 = 500$.

the curves for $n_2 = 50$ and 200 (both with a long chain to short chain ratio of 2:1) are quite close to each other while that for $n_2 = 500$ (5:1) is significantly lower. This suggests that near the Θ-point, $U(r)$ curves for chains of different lengths but the same ratio between the lengths of the chains will be nearly identical.

The potential of mean force can be used to calculate the second osmotic virial coefficient. The virial expansion can be written as

$$P/\rho kT = 1 + B_2\rho + B_3\rho^2 + \ldots \quad (6)$$

where P is the osmotic pressure, ρ is the molecular density of the polymer, k is Boltzmann's constant, T is temperature, and B_2 and B_3 are the second and third osmotic virial coefficients, respectively. The second osmotic virial coefficient, B_2, can be calculated from[11]

$$B_2 = \frac{1}{2}\int \exp^{-U_1/kT-U_2/kT}(1 - \exp^{-U_{12}(r_{12})/kT})\, d\mathbf{r}_{12}\, d\Omega_1\, d\Omega_2 / \int \exp^{-U_1/kT-U_2/kT}\, d\Omega_1\, d\Omega_2 \quad (7)$$

where U_1 and U_2 are the intramolecular potentials of the two single polymer chains, $U_{12}(r_{12})$ is the intermolecular potential between the two chains, the integrals over $d\Omega_1$ and $d\Omega_2$ account for all internal degrees of freedom of the two polymers, and the integral over $d\mathbf{r}_{12}$ is over all separations between the chains' centers of mass. The integration over $d\Omega_1$ and $d\Omega_2$ and the Boltzmann factors associated with the intramolecular potentials are taken into account in the generation of conformations in the pivot algorithm. Thus, with the substitution $d\mathbf{r}_{12} = 4\pi r_{12}^2 dr_{12}$, the equation for B_2 reduces to

$$B_2 = 2\pi\int_0^\infty r_{12}^2(1 - \exp^{-U_{12}(r_{12})/kT})\, dr_{12} \quad (8)$$

Since the potential of mean force $U(r) = U_{12}(r_{12})$, B_2 can be calculated simply by numerical integration using $U(r)$ from the computer simulations presented earlier (Figures 3–11). Calculated second osmotic virial coefficients and the standard error for all combinations of n_1, n_2, and ϵ examined are shown in Table 3. For example, for $n_1 = n_2 = 100$ at $\epsilon = 0.0$ the second osmotic virial coefficient $B_2 = 3026.6 \pm 4.3$. It should be pointed out that the values for B_2 given in this paper are all normalized by the bead diameter cubed, d^3, to account for the distance scale used (i.e. bead diameter is unity). The results are also presented in graphic format in Figures 12–14, which are described in the following paragraphs.

Figure 12 shows the dependence of the second osmotic virial coefficient, B_2/n^2, on chain length, n, for athermal chains. For large n, one expects the second osmotic virial coefficient to have a power law dependence on n of the following form

$$B_2/n^2 \propto (n-1)^{-\gamma} \quad (9)$$

where γ is the scaling exponent.[12] A straight line fit to the $\ln(B_2/n^2)$ versus $\ln(n-1)$ data shown in Figure 12 gives a value of $\gamma = 0.272 \pm 0.005$. For lattice chains, Bellemans and Janssens[17] report $\gamma = 0.278 \pm 0.005$ for $n \leq 40$ and Olaj and Lantschbauer[3] report $\gamma \approx 0.33$ for $50 \leq n \leq 400$. Of greater relevance to this work are the off-lattice simulation results of Yethiraj et al.[26] who report values of γ between 0.293 and 0.337, depending on what length chains are used. Specifically, they report $\gamma = 0.337 \pm 0.007$ for $4 \leq n \leq 128$, $\gamma = 0.313 \pm 0.006$ for $12 \leq n \leq 128$, $\gamma = 0.299 \pm 0.006$ for $24 \leq n \leq 128$, and $\gamma = 0.293 \pm 0.006$ for $32 \leq n \leq 128$. Since our simulations dealt with $50 \leq n \leq 500$, our result of $\gamma = 0.272$ seems to fall in line with these values for shorter chains. Yethiraj et al. also extrapolate their data to obtain a limiting value of the scaling exponent as $n \to \infty$ of $\gamma = 0.25 \pm 0.02$. Our result of $\gamma = 0.272$ falls between this limiting value and the value for their longer chains.

Figure 13 shows the second osmotic virial coefficient for square-well chains of the same length n as a function

Table 3. Second Virial Coefficients

n_1	n_2	$-\epsilon/kT$	second virial coeff, B_2/d^3
50	50	0.0	926.5 ± 0.8
50	50	0.15	662.2 ± 0.8
50	50	0.3	174 ± 4
50	50	0.45	−1730 ● 60
100	100	0.0	3027 ± 4
100	100	0.15	2201 ● 2
100	100	0.3	650 ± 20
200	200	0.0	9977 ● 8
200	200	0.15	7205 ± 7
200	200	0.3	2470 ● 90
500	500	0.0	49300 ● 100
50	25	0.0	525.7 ± 0.5
100	50	0.0	1705 ± 1
100	50	0.15	1224 ± 2
100	50	0.3	336 ± 9
200	100	0.0	5520 ● 10
200	100	0.15	4065 ● 9
200	100	0.3	1270 ± 50
50	10	0.0	261.5 ± 0.3
100	20	0.0	840 ± 1
200	40	0.0	2723 ± 4
500	100	0.0	13140 ● 40
500	100	0.15	9590 ± 50
500	100	0.3	3000 ● 300

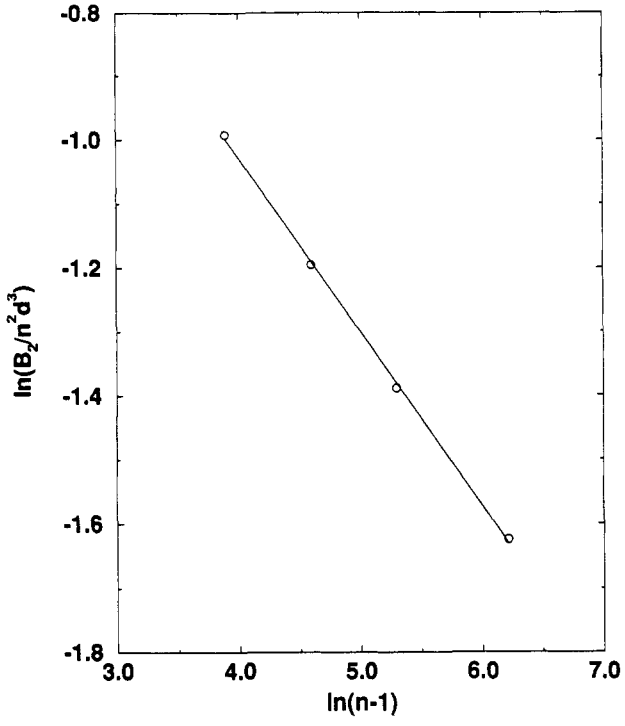

Figure 12. Second osmotic virial coefficient scaling analysis for athermal chains of the same length. The line is the linear fit to the data with the slope −0.272 ± 0.005.

of the bead–bead interaction potential ϵ. From this figure, we can find the Θ-point of the system, which is defined as the point at which the second osmotic virial coefficient is zero. At this point the attractive and repulsive forces (as evidenced by the attractive well and repulsive core in the $U(r)$ curves shown previously) can be said to exactly balance each other. From Figure 13 it can be seen that the Θ-point lies at about $\epsilon_\Theta \cong -0.32kT$ for all chain lengths. This result agrees with the result, $\epsilon_\Theta = -0.325kT$, obtained by Wichert and Hall[27] for short ($n \leq 16$) off-lattice chains. Comparing to lattice chains, this result is quite a bit below the Θ-point of $\epsilon_\Theta = -0.262kT$ reported by Janssens and Bellemans.[18] Clearly, one would not expect the same

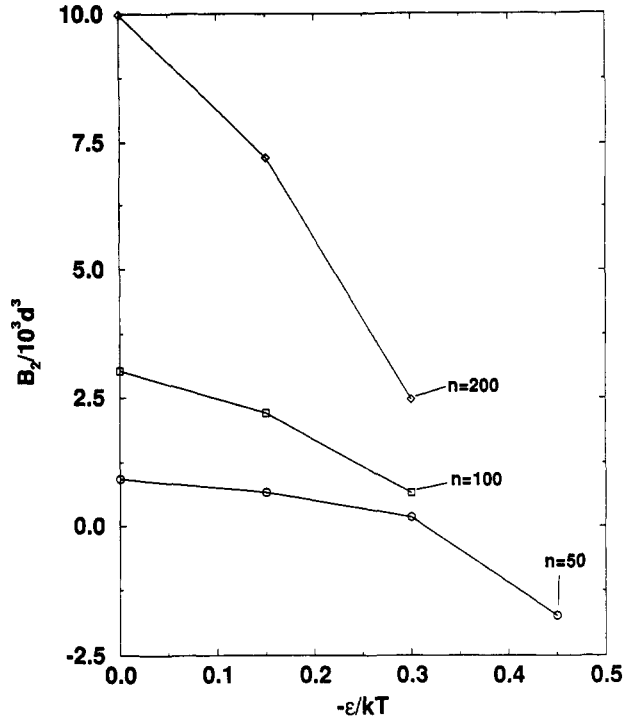

Figure 13. Second osmotic virial coefficient vs $-\epsilon/kT$ for chains of the same length: (○) n = 50, (□) n = 100, and (◇) n = 200.

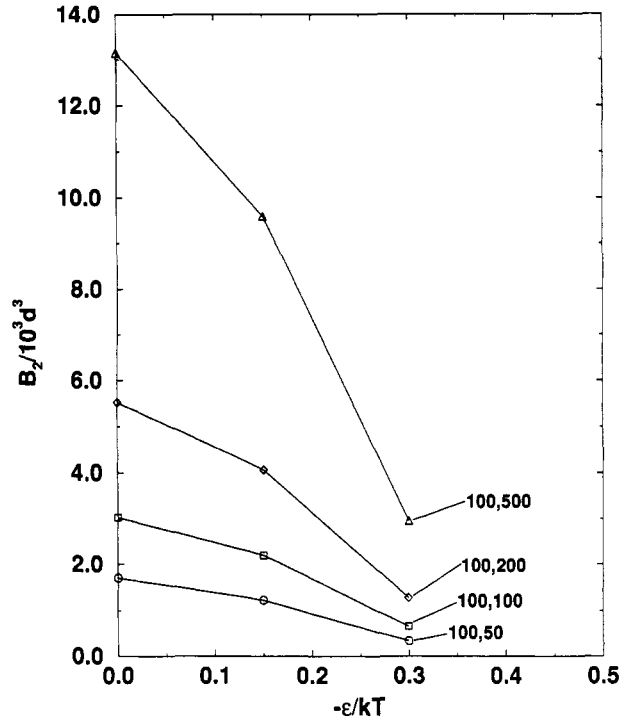

Figure 14. Second osmotic virial coefficient vs $-\epsilon/kT$ for chains of different lengths with n_1 = 100: (○) n_2 = 50, (□) n_2 = 100, (◇) n_2 = 200, and (△) n_2 = 500.

Θ-point for off-lattice and lattice chains since the models are quite different.

Figure 14 shows the second osmotic virial coefficient for a square-well chain of length n_1 = 100 with square-well chains of length n_2 = 50, 100, 200, and 500 as a function of ϵ. In this figure, the same trend shown in Figure 13 is seen regarding the Θ-point, which may be defined as the ϵ where $B_2 = 0$. The second osmotic virial coefficients appear to be converging at a Θ-point of $\epsilon_\Theta \cong -0.32kT$. Additional comparison of Figures 13 and 14 shows that the second osmotic virial coefficient for chains of different lengths lies between the values for chains of the same length

(i.e. B_2 for $n_1 = 100$, $n_2 = 50$ in Figure 14 is between the B_2 values for $n_1 = n_2 = 100$ and $n_1 = n_2 = 50$ in Figure 13). Clearly, this is the expected result.

4. Correlating the Results for $U(r)$

As stated previously, the primary goal of this research is to develop functional forms for the potential of mean force between polymer molecules in dilute solution. The Flory–Krigbaum[9] potential, $U_{FK}(r)$, between two polymers of equal length can be written

$$\frac{U_{FK}(r)}{kT} = n^2 \frac{V_{seg}}{V_{solv}} V_{seg} \left(\frac{3}{4\pi\langle R_g^2\rangle}\right)^{3/2} (1 - 2\chi) \times \exp\left(-\frac{3}{4}\frac{r^2}{\langle R_g^2\rangle}\right) \quad (10)$$

where n is the chain length, V_{seg} is the volume of a polymer segment, V_{solv} is the volume of a solvent molecule, $\langle R_g^2\rangle$ is the mean squared radius of gyration, r is the distance between the centers of mass of the two chains, and χ is given by

$$\chi = \frac{z}{kT}\left[\epsilon_{ps} - \frac{1}{2}(\epsilon_{pp} + \epsilon_{ss})\right] \quad (11)$$

with z equal to the coordination number, ϵ_{ps} equal to the polymer–solvent potential, ϵ_{pp} equal to the polymer–polymer potential, and ϵ_{ss} equal to the solvent–solvent potential. For our square-well model, the solvent–solvent and polymer–solvent interactions are both zero, i.e., $\epsilon_{ss} = \epsilon_{ps} = 0$, and the polymer–polymer potential is equal to our square-well potential, $\epsilon_{pp} = \epsilon$, reducing the χ term to

$$\chi = -\frac{1}{2}\frac{z\epsilon}{kT} \quad (12)$$

with ϵ equal to the square-well potential. (Note that ϵ is negative for attractive interaction, making χ positive for attraction.) Unfortunately, the Flory–Krigbaum potential has two drawbacks, which have been previously noted,[3,6,7] that prevent us from using it to correlate our simulation data. First, since it only has one exponential term, it cannot contain both an attractive well and a repulsive core such as is seen in the simulation data for $U(r)$ at $\epsilon = -0.3kT$. This problem can be alleviated by the addition of other exponential terms such as those of Czech and Hall[14] which allow $U(r)$ curves to have both positive and negative regions. Their equation for $U(r)$ truncated after the first two terms is

$$\frac{U_{CH}(r)}{kT} = \frac{\alpha}{2^{3/2}}(1 - 2\chi)\frac{n^2}{\langle R_g^2\rangle^{3/2}} \exp\left(-\frac{3}{4}\frac{r^2}{\langle R_g^2\rangle}\right) + \frac{\alpha^2}{3^{3/2}}\frac{n^3}{\langle R_g^2\rangle^3} \exp\left(-\frac{r^2}{\langle R_g^2\rangle}\right) \quad (13)$$

with $\alpha = (3/2\pi)^3/2V$ (where $V = \pi/6$, the excluded volume of a polymer segment or solvent molecule). With this form, $U_{CH}(r)$ can have positive and negative regions when one exponential term is positive and the other is negative. The second drawback is that the Flory–Krigbaum potential predicts that, at any given separation, $U(r)$ increases with chain length; this is in contrast to the simulation results shown in Figures 3 and 8 and to those of Grosberg et al.[7] which show that $U(r)$ decreases with increasing chain length. This problem cannot be alleviated by theoretical treatments that merely add additional terms to the Flory–Krigbaum potential (as was done in the paper by Czech and Hall).

Although the Flory–Krigbaum and Czech and Hall models have severe limitations, we can nevertheless borrow some of the ideas contained therein in fitting (or correlating) our data. We do find that an equation of the form

$$\frac{U(r)}{kT} = A \exp\left(-\frac{3}{4}\frac{r^2}{\langle R_g^2\rangle}\right) + B \exp\left(-\frac{r^2}{\langle R_g^2\rangle}\right) \quad (14)$$

can fit our data sets for chains of all lengths quite well. The two exponential terms preserve the basic form of the theoretical equations and the coefficients A and B are found to be functions of n and ϵ. In addition, the A coefficient can include a χ-like term which makes it resemble the theoretical equations even more closely. Olaj et al.[6,15,16] also use two exponential terms, one each for attractive and repulsive interactions between chains, to model $U(r)$; however, they take a somewhat different approach by concentrating on $U(r)$ at the Θ-point. Thus, at least the basic form of the theoretical equations are used in our correlation.

In developing a model that can adequately fit our simulation data on $U(r)$ for chains of the same length, we would like to have a general equation for $U(r)$ that depends only on the chain length, n, and the bead–bead square-well potential, ϵ. For chains of the same length, the two coefficients A and B in the equation above can be fit to the following forms:

$$A = [1 - z(-\epsilon/kT)][a + bn^c + d(-\epsilon/kT)^e] \quad (15)$$

$$B = fn^g + h(-\epsilon/kT)^i \quad (16)$$

The values of A and B for any given n and ϵ were determined by a two-parameter fit over all separations, r, of eq 14 to the $U(r)$ data on chains of the same length presented earlier. The parameters $a - i$ and z can all be obtained by fitting values of A and B from simulation data to the forms given in eqs 15 and 16. Athermal data on chains of all equal lengths and square-well data on chains of the same length $n = 50$ can be used to determine the values of the parameters in the following manner. For athermal chains, $\epsilon = 0.0$, the coefficients A and B reduce to

$$A_{athermal} = a + bn^c \quad (17)$$

$$B_{athermal} = fn^g \quad (18)$$

Fitting the values of A and B for the athermal simulation data shown earlier in Figure 3 to these forms gives values for the parameters a, b, c, f, and g. Once the athermal forms of A and B have been determined, the chain length is held constant at $n = 50$ to determine how A and B depend on ϵ. For square-well chains of length $n = 50$ the result is

$$A_{n=50} = [1 - z(-\epsilon/kT)][A_{athermal,n=50} + d(-\epsilon/kT)^e] = [1 - z(-\epsilon/kT)][2.563 + d(-\epsilon/kT)^e] \quad (19)$$

$$B_{n=50} = B_{athermal,n=50} + h(-\epsilon/kT)^i = 0.3224 + h(-\epsilon/kT)^i \quad (20)$$

Fitting the values of A and B to the square-well simulation data for $n = 50$ shown earlier in Figure 5 gives values for

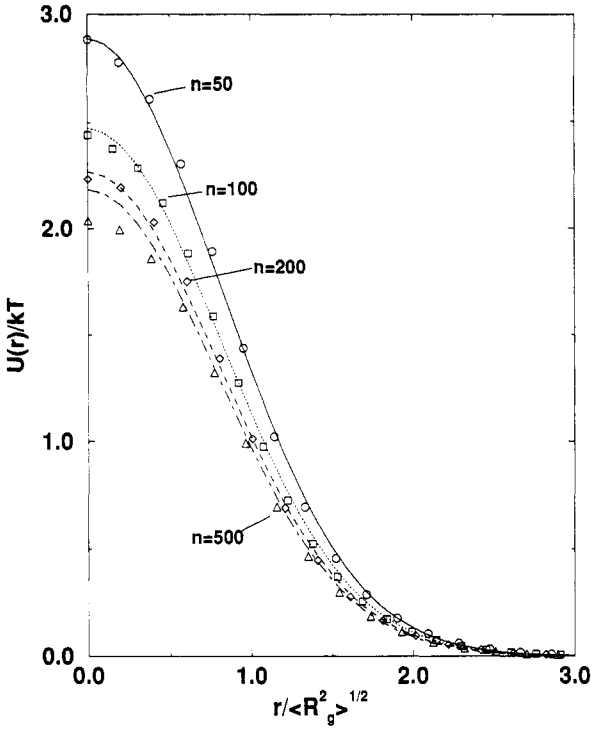

Figure 15. $U(r)$ correlation for athermal chains of the same length: (solid line, ○) $n = 50$, (dotted line, □) $n = 100$, (dashed line, ◇) $n = 200$, and (dot-dashed line, △) $n = 500$. Lines are the correlation and points are the simulation data.

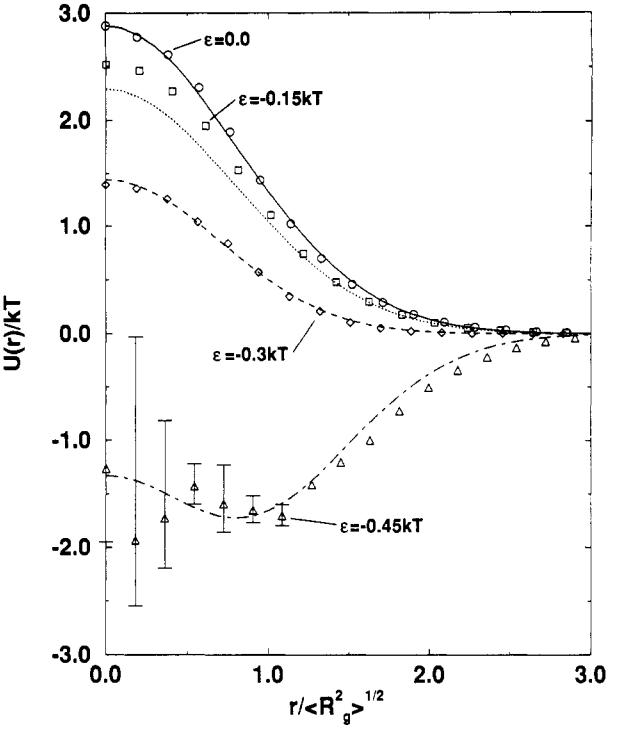

Figure 16. $U(r)$ correlation for chains of length $n = 50$ for varying well depth ϵ: (solid line, ○) athermal, (dotted line, □) $\epsilon = -0.15kT$, (dashed line, ◇) $\epsilon = -0.3kT$, and (dot-dashed line, △) $\epsilon = -0.45kT$. Lines are the correlation and points are the simulation data.

the parameters z, d, e, h, and i. The final correlation for the parameters A and B associated with the expression in eq 14 for the potential of mean force between two polymers of equal size is

$$A = [1 - 3.43(-\epsilon/kT)][1.38 + 21.4n^{-0.740} + 117(-\epsilon/kT)^{2.34}] \quad (21)$$

$$B = 0.116n^{0.261} + 421(-\epsilon/kT)^{4.74} \quad (22)$$

Although this correlation is developed using only part of our simulation data, it does a reasonable job of fitting all of our data for chains of the same length.

Figure 15 shows how well the athermal version of the $U(r)$ correlation (eqs 14, 21, and 22) fits the simulation data for $U(r)$ versus r shown previously in Figure 3. The lines show the correlation calculations for the given n and ϵ, while the points are the simulation data. It can be seen that the model fits the data extremely well for $n = 50$, 100, and 200 over the whole range of seqarations and is only slightly high for $n = 500$ at very short distances of separation. Since the athermal data were used to fit the parameters of the correlation coefficients A and B, the good fits of the correlation to the data are not surprising.

Figure 16 shows how well the correlation fits the $U(r)$ simulation data for square-well chains of length $n = 50$ shown earlier in Figure 5. Again, the lines show the correlation calculations and the points are the simulation data. The correlation fits very well for $\epsilon = 0.0$ and $-0.3kT$ over the whole range of separations. For the $\epsilon = -0.15kT$ case, the correlated value of $U(r)$ is a bit below the simulation data at short distances. Again, these fits are not surprising as the data for square-well chains of length $n = 50$ were used in fitting the correlation coefficients A and B. Interestingly, the correlation does a reasonable job for $\epsilon = -0.45kT$ even though the data are not particularly good.

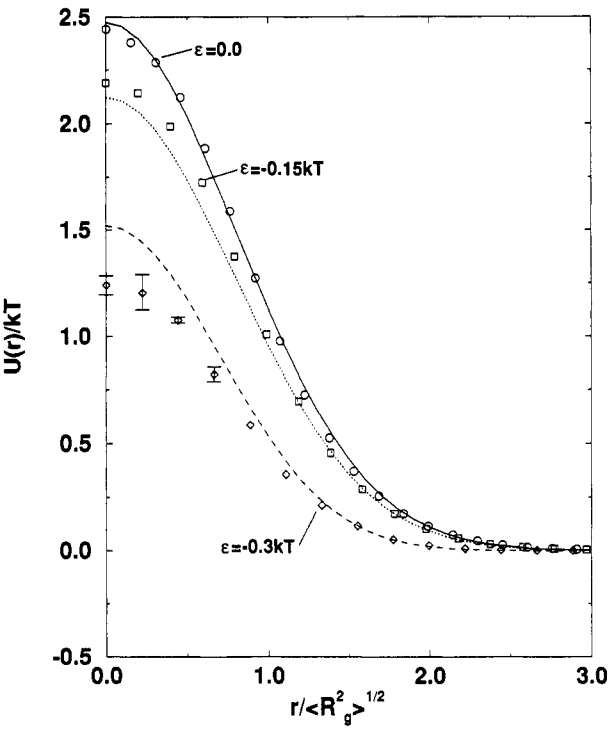

Figure 17. $U(r)$ correlation for chains of length $n = 100$ for varying well depth ϵ: (solid line, ○) athermal, (dotted line, □) $\epsilon = -0.15kT$, and (dashed line, ◇) $\epsilon = -0.3kT$. Lines are the correlation and points are the simulation data.

Figures 17 and 18 show how the correlation for $U(r)$ fits the simulation data for square-well chains of length $n = 100$ (from Figure 6) and $n = 200$ (from Figure 7), respectively. Since the correlation was developed using only athermal data for both of these chain lengths, the real test of its usefulness is to see how well it fits the square-well simulation data for $n = 100$ and $n = 200$. In Figure 17 for $n = 100$ it can be seen that the correlation fits the $\epsilon = -0.15kT$ data quite well, being only slightly low at

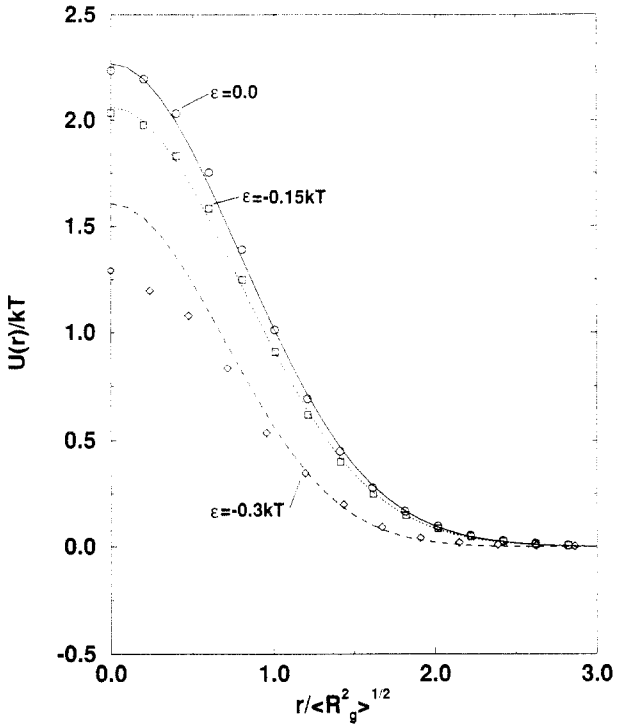

Figure 18. $U(r)$ correlation for chains of length $n = 200$ for varying well depth ϵ: (solid line, ○) athermal, (dotted line, □) $\epsilon = -0.15kT$, and (dashed line, ◇) $\epsilon = -0.3kT$. Lines are the correlation and points are the simulation data.

short distances of separation. The $U(r)$ correlation for $n = 100$, $\epsilon = -0.3kT$ lies above the simulation data but is still fairly good. For the $n = 200$ data shown in Figure 18, the correlation fits the $\epsilon = -0.15kT$ almost exactly, but as was the case for $n = 100$, the correlation for $\epsilon = -0.3kT$ is higher than the simulation data.

For chains with a length ratio of 2:1 (e.g. $n_1 = 100$, $n_2 = 50$), an analysis similar to the one described above can be employed. Again using the form of $U(r)$ given in eq 14, the coefficients A and B can be fit to the following forms:

$$A = [1 - z(-\epsilon/kT)][a + b(\sqrt{n_1 n_2})^c + d(-\epsilon/kT)^e] \quad (23)$$

$$B = j + f(\sqrt{n_1 n_2})^g + h(-\epsilon/kT)^i \quad (24)$$

It can be seen that the only differences between these forms for A and B and those given in eqs 15 and 16 are the substitution of $\sqrt{n_1 n_2}$ for n and the addition of a constant, j, to the B term. Unfortunately, this $U(r)$ correlation for chains with a 2:1 length ratio does not reduce to the $U(r)$ correlation for chains of the same length when $n_1 = n_2$, so the values of the parameters $a - j$ and z must be redetermined. When the method given earlier for chains of the same length was followed, A and B were determined by fitting eq 14 to $U(r)$ curves for chains with a 2:1 length ratio. The A and B values for athermal chains and square-well chains of length $n_1 = 100$, $n_2 = 50$ were fit to the forms given in eqs 23 and 24 to obtain values for the parameters $a - j$. It should be noted here that the value of the parameter z was taken to be 3.43 (the value determined for chains of the same length) because it is essentially a "coordination number" for the model and should not depend on the ratio of chain lengths. The final correlation for the coefficients A and B associated with eq 14 for the potential of mean force between chains with a 2:1 length ratio is

$$A = [1 - 3.43(-\epsilon/kT)][1.42 + 33.1(\sqrt{n_1 n_2})^{-1.17} + 281(-\epsilon/kT)^{2.95}] \quad (25)$$

$$B = 0.599 + 117(\sqrt{n_1 n_2})^{-1.78} + 26.9(-\epsilon/kT)^{2.91} \quad (26)$$

This correlation does a good job of fitting our simulation data for chains with a 2:1 length ratio.

Figures 19–21 show how the $U(r)$ correlations described above fit our simulation data for chains with a 2:1 length ratio. Figure 19 shows how well the correlation in eqs 14, 25, and 26 fits our simulation data on $U(r)$ for athermal chains of lengths $n_1 = 50$, $n_2 = 25$; $n_1 = 100$, $n_2 = 50$; and $n_1 = 200$, $n_2 = 100$. Figure 20 shows how well this correlation fits our simulation data on $U(r)$ for square-well chains of length $n_1 = 100$, $n_2 = 50$. Figure 21 shows how well the correlation fits our simulation data on $U(r)$ for square-well chains of length $n_1 = 200$, $n_2 = 100$. It can be seen from all of these figures that the correlation for chains with a 2:1 length ratio does an excellent job of fitting our $U(r)$ simulation data.

For chains with a length ratio of 5:1 (e.g. $n_1 = 500$, $n_2 = 100$), an analysis similar to the one described above fails due to the fact that the A and B values found by fitting eq 14 to the simulation data cannot be reproduced by equations with the same form as eqs 23 and 24. In particular, the A and B values for the square-well simulation data at $n_1 = 500$, $n_2 = 100$ do not follow the same pattern that was noticed for chains of the same length or for chains with a 2:1 length ratio (i.e. the A and B values for 5:1 square-well chains did not uniformly increase or decrease as functions of ϵ). For athermal chains with a 5:1 length ratio, the values of A and B can be fit by equations with the form of eqs 17 and 18 if we replace n with $\sqrt{n_1 n_2}$ and determine new values for the parameters a, b, c, f, and g. For square-well chains with a length ratio of 5:1, the values of A and B can be fit by equations with the form of eqs 19 and 20 if we change the values of A and B (keeping $A + B$ constant) such that they uniformly increase or decrease as functions of ϵ and use the previously determined value of z. Postulating the A and B values for square-well chains in this manner allows the following correlation for chains with a 5:1 length ratio to be determined.

$$A = [1 - 3.43(-\epsilon/kT)][-0.529 + 4.91(\sqrt{n_1 n_2})^{-0.307} + 0.326(-\epsilon/kT)^{0.001}] \quad (27)$$

$$B = 0.0907(\sqrt{n_1 n_2})^{0.410} + 0.443(-\epsilon/kT)^{0.882} \quad (28)$$

Again, it should be noted that this correlation is not the same as either the correlation for chains with a 2:1 length ratio or the correlation for chains of the same length. Although this correlation was not derived from actual A and B fits to the simulation data for square-well chains, the correlation still does a reasonable job of fitting our simulation data for chains with a 5:1 length ratio.

Figures 22 and 23 show how the $U(r)$ correlation in eqs 14, 27, and 28 fits our simulation data for chains with a 5:1 length ratio. Figure 22 shows how well the correlation fits our simulation data on $U(r)$ for athermal chains of lengths $n_1 = 50$, $n_2 = 10$; $n_1 = 100$, $n_2 = 20$; $n_1 = 200$, $n_2 = 40$; and $n_1 = 500$, $n_2 = 100$. One would expect a good fit of the correlation to athermal data since the actual values of A and B for athermal chains were used in developing the correlation. Figure 23 shows how well the correlation fits our simulation data on $U(r)$ for square-

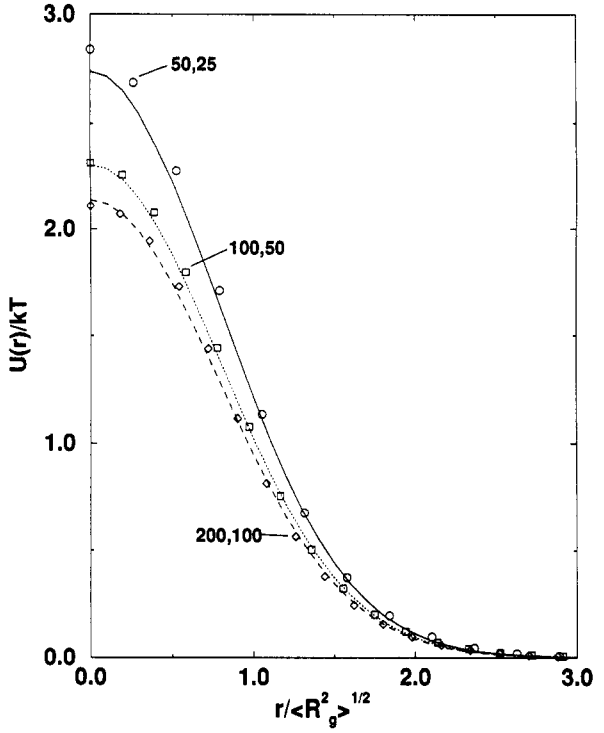

Figure 19. $U(r)$ correlation for athermal chains with a 2:1 ratio of lengths: (solid line, ○) $n_1 = 50$, $n_2 = 25$; (dotted line, □) $n_1 = 100$, $n_2 = 50$; and (dashed line, ◇) $n_1 = 200$, $n_2 = 100$. Lines are the correlation and points are the simulation data.

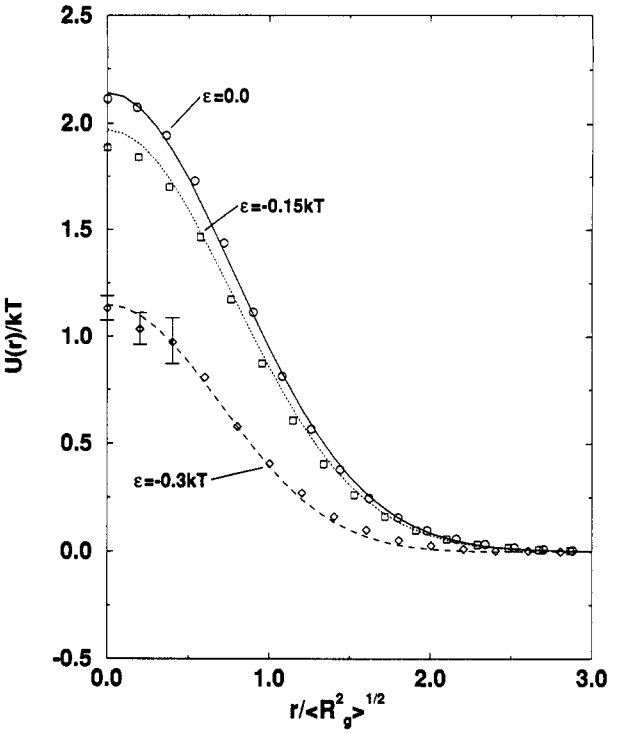

Figure 21. $U(r)$ correlation for chains of length $n_1 = 200$, $n_2 = 100$ for varying well depth ϵ: (solid line, ○) athermal, (dotted line, □) $\epsilon = -0.15kT$, and (dashed line, ◇) $\epsilon = -0.3kT$. Lines are the correlation and points are the simulation data.

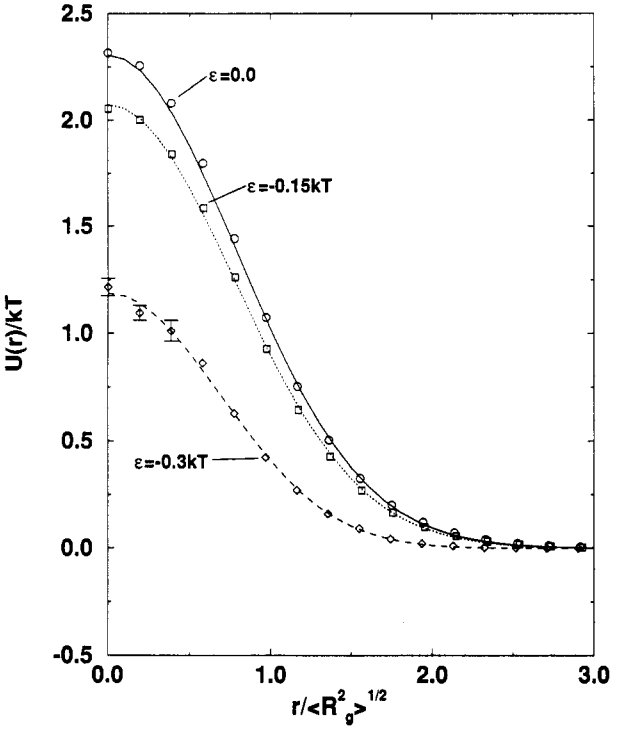

Figure 20. $U(r)$ correlation for chains of length $n_1 = 100$, $n_2 = 50$ for varying well depth ϵ: (solid line, ○) athermal, (dotted line, □) $\epsilon = -0.15kT$, and (dashed line, ◇) $\epsilon = -0.3kT$. Lines are the correlation and points are the simulation data.

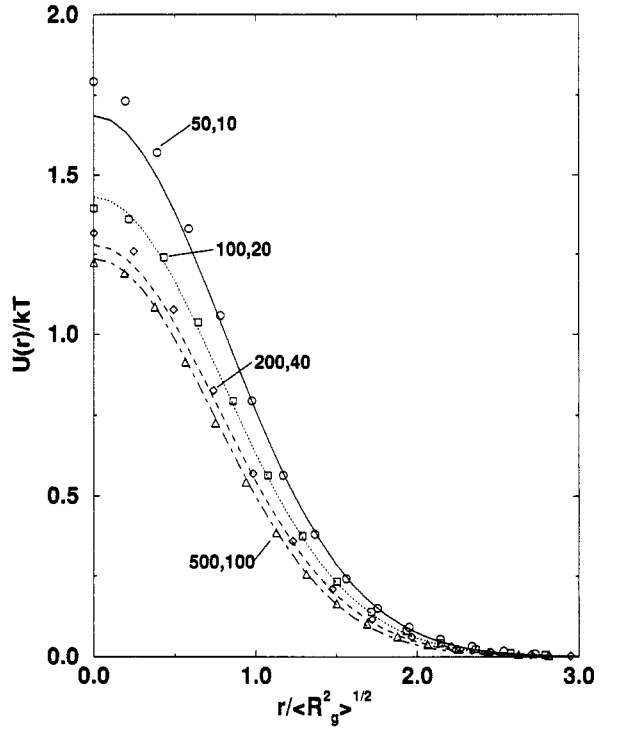

Figure 22. $U(r)$ correlation for athermal chains with a 5:1 ratio of lengths: (solid line, ○) $n_1 = 50$, $n_2 = 10$; (dotted line, □) $n_1 = 100$, $n_2 = 20$; (dashed line, ◇) $n_1 = 200$, $n_2 = 40$; and (dot-dashed line, △), $n_1 = 500$, $n_2 = 100$. Lines are the correlation and points are the simulation data.

well chains of length $n_1 = 500$, $n_2 = 100$. The good fit between the correlation and the square-well simulation data is surprising considering that the best-fit A and B values to eq 14 for the square-well chains were changed so that they would uniformly increase or decrease with ϵ. It can be seen from the figures that the correlation for chains with a 5:1 length ratio does a reasonably good job of fitting our $U(r)$ simulation data.

The basic form of a correlation for $U(r)$ is given by eqs 14–16. For each length ratio studied (1:1, 2:1, and 5:1), the values of the parameters used to calculate A and B were determined. For chains with a length ratio of 1:1, eqs 21 and 22 are the correlations for A and B. For chains with a length ratio of 2:1, eqs 25 and 26 are the correlations for A and B. For chains with a length ratio of 5:1, eqs 27 and 28 are the correlations for A and B. Although the

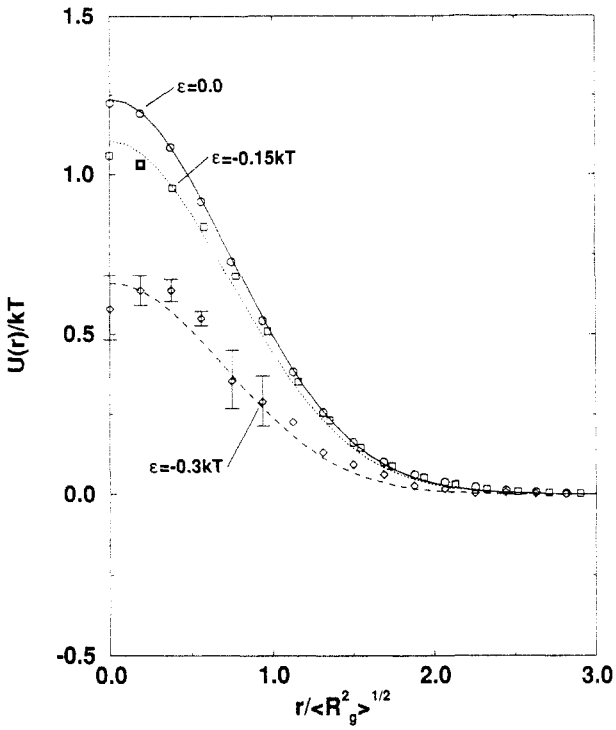

Figure 23. $U(r)$ correlation for chains of length $n_1 = 500$, $n_2 = 100$ for varying well depth ϵ: (solid line, ○) athermal, (dotted line, □) $\epsilon = -0.15kT$, and (dashed line, ◇) $\epsilon = -0.3kT$. Lines are the correlation and points are the simulation data.

correlations for chains of different lengths do not reduce to the correlation for chains of the same length when $n_1 = n_2$, the fact that correlations with the same basic form can fit all of our simulation data lends some hope that a truly general correlation for $U(r)$ can eventually be developed. Overall, the individual correlations seem to do quite a good job of fitting all of our simulation data.

5. Conclusion

In the work presented in this paper, polymers were modeled by off-lattice chains of tangent hard spheres of length $n = 50, 100, 200$, and 500 for both the athermal case ($\epsilon = 0.0$) and the case where the beads of the chain have attractive potentials. The attractive potential was modeled as a square-well potential with well depth $\epsilon = -0.15kT$, $-0.3kT$, and $-0.45kT$ and well width $\lambda = 0.5$. Single chain conformations were generated using the pivot algorithm. Two sets of single chain conformations were used to create two-chain configurations which were used to examine the interaction between chains.

The radius of gyration, the potential of mean force between two chains, and the second osmotic virial coefficient were all examined. The radius of gyration of single chains was used to find the Θ-point, which can be defined as the ϵ where $R_g^2 \propto n$, at $\epsilon_\Theta \cong -0.32kT$. Results for the potential of mean force, $U(r)$, between chains of the same length showed that for a given bead–bead potential $U(r)$ decreases with increasing chain length. Although this is contrary to the Flory–Krigbaum theory[9] prediction, it is in agreement with the findings of Grosberg et al.[7] $U(r)$ between chains of a given length was also seen to decrease as ϵ decreased. For chains of different lengths, $U(r)$ was lower than for chains of the same length. In addition, as the difference in the length of the chains increased, the difference between $U(r)$ for chains of different lengths and chains of the same length increased. The $U(r)$ curves for both same and different length chains converged near the Θ-point. Scaling analysis of the second osmotic virial coefficient for athermal chains gave a scaling exponent of $\gamma = 0.272 \pm 0.005$. This result falls in well with the findings of Yethiraj et al.[26] Examination of the second osmotic virial coefficient for square-well chains gave a Θ-point, which can be defined as the ϵ where $B_2 = 0$, at $\epsilon_\Theta \cong -0.32kT$. This is the same Θ-point found for single chains and is in agreement with the findings of Wichert and Hall.[27] A correlation for $U(r)$ which does a reasonable job of fitting all of our simulation data was also presented.

Acknowledgment. We would like to thank Dr. Rainer Czech for suggesting this work to us and helping us to begin the computations. This material is based upon work partially supported under a National Science Foundation Graduate Fellowship. Additional support for this work was provided by NSF Grant Nos. CTS-9208590 and CBT-8720284 and North Carolina Biotechnology Center Grant No. 9113-ARG-0205.

References and Notes

(1) Bishop, M.; Clarke, J. H. R. *J. Chem. Phys.* **1991**, *94*, 3936.
(2) Yuan, X.-F.; Masters, A. J. *J. Chem. Phys.* **1991**, *94*, 6908.
(3) Olaj, O. F.; Lantschbauer, W. *Ber. Bunsen-Ges. Phys. Chem.* **1977**, *81*, 985.
(4) Olaj, O. F.; Lantschbauer, W.; Pelinka, K. H. *Macromolecules* **1980**, *13*, 299.
(5) Olaj, O. F.; Zifferer, G. *Makromol. Chem.* **1983**, *184*, 2619.
(6) Olaj, O. F.; Pelinka, K. H. *Makromol. Chem.* **1976**, *177*, 3413.
(7) Grosberg, A. Y.; Khalatur, P. G.; Khokhlov, A. R. *Mackromol. Chem., Rapid Commun.* **1982**, *3*, 709.
(8) Krüger, B.; Schäfer, L.; Baumgärtner, A. *J. Phys. Fr.* **1989**, *50*, 3191.
(9) Flory, P. J.; Krigbaum, W. R. *J. Chem. Phys.* **1950**, *18*, 1086.
(10) Flory, P. J. *Principles of Polymer Chemistry*; Cornell University Press: Ithaca, NY, 1953.
(11) Yamakawa, H. *Modern Theory of Polymer Solutions*; Harper and Row: New York, 1971.
(12) DeGennes, P.-G. *Scaling Concepts in Polymer Science*; Cornell University Press: Ithaca, NY, 1979.
(13) Freed, K. F. *Renormalization Group Theory of Macromolecules*; John Wiley & Sons: New York, 1987.
(14) Czech, R.; Hall, C. K. *Macromolecules* **1991**, *24*, 1535.
(15) Olaj, O. F. *Makromol. Chem.* **1976**, *177*, 3427.
(16) Olaj, O. F.; Zifferer, G.; Rhemann, H. *Monatsh. Chem.* **1985**, *116*, 1395.
(17) Bellemans, A.; Janssens, M. *Macromolecules* **1974**, *7*, 809.
(18) Janssens, M.; Bellemans, A. *Macromolecules* **1976**, *9*, 303.
(19) Öttinger, H. C. *Macromolecules* **1985**, *18*, 93.
(20) Poland, D. *Macromolecules* **1991**, *24*, 3352.
(21) Barrett, A. J. *Macromolecules* **1985**, *18*, 196.
(22) Yato, H.; Okamoto, H. *Macromolecules* **1990**, *23*, 3459.
(23) Bruns, W. *Macromolecules* **1984**, *17*, 2826.
(24) Meirovitch, H.; Lim, H. A. *J. Chem. Phys.* **1990**, *92*, 5144.
(25) Meirovitch, H.; Lim, H. A. *J. Chem. Phys.* **1990**, *92*, 5155.
(26) Yethiraj, A.; Honnell, K. G.; Hall, C. K. *Macromolecules* **1992**, *25*, 3979.
(27) Wichert, J.; Hall, C. K. *Macromolecules* **1994**, *27*, 2744.
(28) Kremer, K.; Binder, K. *Comput. Phys. Rep.* **1988**, *7*, 259.
(29) Lal, M. *Mol. Phys.* **1969**, *17*, 57.